A 'TRANS' ANALYSIS OF EFFECTS OF LORENTZ FORCE AND WALL TOPOLOGY ON THE REORGANISATION OF COHERENT STRUCTURES IN R-B CONVECTION

S. Kenjereš and K. Hanjalić
Thermofluids Section, Department of Applied Physics, Delft University of Technology
Lorentzweg 1, 2628 CJ Delft, The Netherlands

ABSTRACT

The paper reports on recent progress in the application of Time-dependent Reynolds-averaged Navier-Stokes (TRANS) approach to the analysis of the effect of magnetic force and bottom wall configuration on the reorganisation of large coherent structure in Rayleigh-Bénard (R-B) convection. Based on 'triple decomposition', the large scale periodic motion is fully resolved in time and space, whereas the unresolved random motion is modelled using the conventional algebraic flux expressions closed with the low-Re-number $k-\varepsilon-\overline{\theta^2}$ three-equation model. The applied method reproduced the major features of the coherent structure, as well as the long-term first and second moments in accord with the available DNS results.

INTRODUCTION

In many turbulent flows of industrial relevance large-scale coherent structures are the major carrier of momentum, heat and species. In such cases the transport processes can best be controlled by affecting coherent eddy structure, either by imposing an external force (*distributed* control), or by control of *boundary* topology or its physical conditions (surface heat and mass transfer). Both techniques have long been in use: rotation, buoyancy, electric or magnetic field, surface blowing or suction, riblets and grooves, are only some of the means applied to control drag, heat and mass transfer, entrainment and mixing, combustion, noise. However, it is only recently, with the advancement of experimental field techniques (e.g. PIV) and of Direct Numerical and Large Eddy Simulations (DNS, LES), that the flow and turbulence control studies focus more on coherent structure. Major prerequisites for such an approach are the ability to identify organised structures and a proper interpretation of their role in controlling the flow and transport processes. While DNS and LES methods can provide necessary information, their application in complex industrial flows at higher Reynolds numbers is still not feasible. On the other hand, the conventional Reynolds-averaged Navier-Stokes (RANS) approach, which is still used as a major industrial predictive tool, conceals by its virtue any spectral information, and is regarded as unsuitable for detecting any identifiable eddy structure.

In this paper we argue that for flows with a dominant large eddy structure (vortex shedding, shear layers, longitudinal vortices, Rayleigh-Bénard convection), the application of time-dependent RANS ('TRANS') can be a useful tool in identifying the organised motion and its response to the imposed distributed or boundary control. The approach is akin to Very large Eddy Simulation (VLES) by which the large structure is fully resolved, whereas the 'rest' of turbulence is modelled by conventional turbulence closure models ('subscale model'). As compared to LES, both contributions to the long-term statistical averages are of equal order of magnitude. Close to a solid wall, the unresolved (modelled) part is more dominant, which imposes requirements to model accurately the wall phenomena. On the other hand, the resolved motion recovers the large scale transport, which in conventional RANS is usually modelled *inadequately* by gradient hypotheses.

In order to justify the TRANS approach we investigate several cases of steady Rayleigh-Bénard convection, in which large scale coherent structure is known to exist, and for which DNS and experimental data are available. Comparison of TRANS and DNS statistics, which serves as a first check if the TRANS approach is meaningful, requires a care in the interpretation of the statistics in order to account for the contribution of the resolved motion. The triple decomposition, by which the instantaneous field is assumed to consist of long term average (time-mean), periodic (large-scale structure) and random, provides a satisfactory tool, indicating that the long-term statistics can be well reproduced by accounting for both the random and periodic contributions. A second test of applicability of TRANS is the comparison of structure identification functions evaluated in parallel from DNS and TRANS realizations. Various identification criteria have been applied including numerical visualisation, critical point and vortex dynamics approaches.

EQUATIONS AND MODEL

The instantaneous motion of a conductive fluid under the joint action of buoyancy and magnetic force is described by the equations for momentum, energy and

electric potential:

$$\frac{\partial \hat{U}_i}{\partial t} = \frac{\partial}{\partial x_j}\left(\nu\frac{\partial \hat{U}_i}{\partial x_j} - \hat{U}_i\hat{U}_j\right) - \frac{1}{\rho}\frac{\partial \hat{P}}{\partial x_i} + \beta g_i \Delta\hat{T} + \underbrace{\sigma(\epsilon_{ijk}\hat{B}_k\frac{\partial \hat{\Phi}}{\partial x_j} + \hat{U}_k\hat{B}_i\hat{B}_k - \hat{U}_i\hat{B}_k^2)}_{\hat{F}_i^L} \quad (1)$$

$$\frac{\partial \hat{T}}{\partial t} = \frac{\partial}{\partial x_j}\left(\alpha\frac{\partial \hat{T}}{\partial x_j} - \hat{T}\hat{U}_j\right) \quad (2)$$

$$\nabla^2\Phi = \nabla\cdot\mathbf{U}\times\mathbf{B} \quad (3)$$

where $\hat{F}_i^L$ is the Lorentz force, $\hat{\Phi}$ is the electric potential and $\hat{B}_i$ is the imposed magnetic field.

Assuming that the large scale structure is distinctly separated in the spectral space from the rest of turbulence, we can decompose the instantaneous flow property at a point $\hat{\Phi}(x_i,t)$ into time-mean $\overline{\Phi}(x_i)$, periodic $\tilde{\Phi}(x_i,t)$ and random $\phi(x_i,t)$, i.e.

$$\hat{\Phi}(x_i,t) = \overline{\Phi}(x_i) + \tilde{\Phi}(x_i,t) + \phi(x_i,t).$$

By performing a long-term time averaging at a point in space and assuming that because of a spectral gap in between, the periodic and random motion are not directly interacting, the second moments are obtained as a sum of the resolved and modelled contributions, as follows from the long-term averaging, i.e. for variables Φ and Ψ :

$$\overline{\hat{\Phi}\hat{\Psi}} - \overline{\Phi}\overline{\Psi} = \overline{\tilde{\Phi}\tilde{\Psi}} + \overline{\phi\psi} \quad (4)$$

Unlike in LES, both contributions are usually of the same order of magnitude and close to a wall the unresolved part is often larger, as it is shown later in the case of the turbulent heat flux and temperature variance.

In order to illustrate the implication of the approach we consider the long-term averaged energy equation, which for steady R-B convection reduces to:

$$\frac{\partial}{\partial x_j}\left(\alpha\frac{\partial \overline{T}}{\partial x_j} - \overline{TU_j} - \overline{\tilde{T}\tilde{U}_j} - \overline{\theta u_j}\right) = 0 \quad (5)$$

The first three terms are provided from TRANS and the last term from the single-point model. Further averaging over homogeneous (horizontal) planes yields the expression for the total heat flux in vertical direction (z)

$$\alpha\frac{\partial \overline{T}}{\partial z} - \overline{\tilde{T}\tilde{W}} - \overline{\theta w} = \frac{q_w}{\rho c_p} = const. \quad (6)$$

The contribution of the unresolved motion to the heat flux $-\overline{\theta u_j}$ is modelled by a 'reduced' algebraic flux/stress model derived from the modelled differential transport equation for $\overline{\theta u_i}$ by assuming weak equilibrium, but retaining all major flux production terms:

$$\overline{\theta u_i} = -C\frac{k}{\varepsilon}\left[\overline{u_iu_j}\frac{\partial \tilde{T}}{\partial x_j} + \xi\overline{\theta u_j}\frac{\partial \tilde{U}_i}{\partial x_j} + \eta(\beta g_i\overline{\theta^2} + \overline{\theta f_i^L})\right] \quad (7)$$

where $f_i^L = \mathbf{j}\times\mathbf{B} = \frac{\sigma}{\rho}(\underbrace{-\nabla\phi_e}_{\mathbf{e}} + \mathbf{u}\times\mathbf{B})\times\mathbf{B}$ (8)

is the fluctuating Lorentz force and $\mathbf{e}$ is the fluctuating electric field. Note that bold symbols denote vectors, and $\mathbf{B}$ stands for $\hat{\mathbf{B}} = \overline{\mathbf{B}}$, assumed independent of (or slowly varying with)time.

The turbulent stress tensor $\overline{u_iu_j}$ and the correlations involving the electric field $\overline{u_ie_j}$ and $\overline{\theta e_j}$ can also be expressed in similar algebraic forms by truncation of the full transport equations. However, in the present work we use simple eddy diffusivity expressions for these moments and account for the buoyancy and magnetic field by additional terms in the transport equations for the turbulence kinetic energy k and its dissipation rate ε, Kenjereš and Hanjalić (1999).

$$\frac{\mathrm{D}k}{\mathrm{D}t} = \mathcal{D}_k + P_k + G_k^g + G_k^L - \varepsilon \quad (9)$$

$$\frac{\mathrm{D}\varepsilon}{\mathrm{D}t} = \mathcal{D}_\varepsilon + P_{\varepsilon 1} + P_{\varepsilon 2} + G_\varepsilon^g + G_\varepsilon^L - Y \quad (10)$$

where $G_k^L = -\frac{\sigma}{\rho}B_0^2\, k\, exp\left(-C_L\frac{\sigma}{\rho}B_0^2\frac{k}{\varepsilon}\right)$ (11)

$$G_\varepsilon^L = -\frac{\sigma}{\rho}B_0^2\, \varepsilon\, exp\left(-C_L\frac{\sigma}{\rho}B_0^2\frac{k}{\varepsilon}\right) \quad (12)$$

with C_L=0.025. Other terms in the k and ε equations are modelled in the conventional manner. These two equations, together with the equations for temperature variance $\overline{\theta^2}$ (all modified for low-Re-number and near-wall effects), close the problem, resulting in a three-equation model k–ε–$\overline{\theta^2}$.

The equation set is solved numerically using a finite volume Navier-Stokes solver for three-dimensional flows in structured non-orthogonal geometries, with Cartesian vector and tensor components and collocated variable arrangement. The second order accurate central difference scheme (CDS) was applied for discretisation of diffusive terms and second order linear-upwind or central scheme (LUDS/CDS) for convective terms. The time marching is performed by fully implicit second order three-time-level method which allows larger time steps to be used, in view of the fact that only large scales are being resolved. Typical computations covered about 200-400 nondimensional time units $\tau^*=\tau\sqrt{\beta g\Delta T H}/H$ which correspond roughly to 15-30 convective time scales based on convective velocity and characteristic cell circumference, Kerr (1996).

RESULTS AND DISCUSSION

The TRANS computations of Rayleigh-Bénard convection over a heated flat bottom wall at a range of Rayleigh numbers by Kenjereš and Hanjalić (1998) reproduced very well the mean temperature, wall heat transfer and the second moments obtained by experiments and DNS. An illustration of TRANS performance is given in Fig. 1a, which shows the near-wall blow up of the predicted long-term averaged temperature profiles for three values of Ra number, 6.5×10^6, 10^7 and 10^9.

The results for the two lower Ra numbers are in excellent agreement with available DNS. Moreover, the parallel application of several structure identification methods (second invariant of the velocity gradient, discriminant of its characteristic equation, kinematic vorticity number, massless particle trajectories) to the instantaneous fields obtained by DNS and TRANS showed a striking resemblance in the large structure, including the spiralling updrafts as major constituents of the large scale unsteady roll-cell pattern, Cortese and Balachandar (1993). These findings ensured a confidence in the TRANS approach and its extrapolation to cases with multiple body forces and complex wall topology, which are both expected to impose a reorganisation and modification of the large coherent structure. Because this structure provides major 'communication' between the boundary layers at the bottom and top walls, its modification is expected to influence the overall heat transfer.

R-B convection subjected to Lorentz force. The first case considered is an example of *distributed* turbulence control: a magnetic field imposed on the flow of conductive fluid generates the Lorentz force, which damps the velocity and its fluctuations in the direction of the force, Mößner and Müller (1999). As a consequence, the vortical structure is modified with a tendency to align the major vortex axis with the direction of the magnetic field vector. This effect is utilised currently in controlling the process of metal casting and is regarded as a potential tool to control crystal growth. An algebraic turbulence model has been developed which reproduces well the effect of magnetic field on mean velocity and turbulence stresses in forced turbulent flow in a plane and a square channel, Kenjereš and Hanjalić (1999).

In this paper we analyse a case of magnetic Rayleigh-Bénard convection (RBM), i.e. the situation where the gravitational vector and imposed magnetic field are aligned. The considered Ra number, 10^7, ensures a fully turbulent regime in the absence of magnetic field, enabling thus far the study of the effect of Lorentz force on the reorientation of the vortical structure and the associated transport phenomena. We consider three cases corresponding to zero, medium and a strong magnetic field, defined by Hartman number Ha=0, 20 and 100. Fig. 1b shows the influence of the strength of the imposed magnetic fields on the time evolution of Nu number (all starting with a uniform fluid temperature subjected to a step temperature elevation of the bottom wall). Obviously, the magnetic field significantly damps the heat transfer. It is interesting to note that this damping does not scale linearly with strength of imposed magnetic field. The long-time averaged vertical temperature profiles for the three cases considered are presented in Fig. 1c, showing a visible temperature inversion at strong magnetic field, Ha=100.

Fig. 2a shows the effects of the imposed magnetic field on planform structures (identified by the temperature isosurfaces). Due to Lorentz force in x-y plane (since the imposed magnetic field is oriented in vertical z direction), the horizontal movement of thermal plumes is significantly reduced. At the same time, the thermal plumes are significantly smaller and more extended in vertical direction. The coherent structures, identified by the contours of constant kinematic vorticity number, show a very similar behaviour, Fig. 3. With an increase in Ha number, this structure becomes smaller, with a higher concentration in the near wall regions, and a more pronounced orientation in vertical direction.

Beside the direct effect on large-scale motion (Lorentz force in momentum equations), it is recalled that the additional 'magnetic' terms representing the effects of magnetic field are also present in the model equations for turbulent kinetic energy and its dissipation rate, as well as in the model expression for other second moments. In order to illustrate the relative magnitude of the modelled and resolved contributions to the second moments - within the framework of TRANS approach, Fig. 2b. shows both contributions to the turbulent heat flux and temperature variance for three values of Ha number. As seen, the modelled parts are the main contribution in the near-wall regions ($0<z/D\leq 0.1$, $0.9\leq z/D<1$) for the situation without magnetic field, i.e. Ha=0. When the magnetic field is active, the 'magnetic terms' in the model of the unresolved motion become more important and damp the modelled contribution relative to the resolved one. For Ha=20, both contributions are equally important in the near-wall regions for both $\overline{w\theta}$ and $\overline{\theta^2}$. A further increase in magnet strength leads to a drastic reduction in the modelled contribution, which becomes negligible at Ha=100. It is interesting to note the peaks of the temperature variance $\overline{\theta^2}$ for the largest value of Ha are moved towards the cavity centre, which is a feature of low Ra numbers, indicating a low turbulence intensity.

Effects of Wall Topology. As an example of *boundary controlled structure*, we consider a high Ra number (up to $Ra=10^9$) R-B convection over heated wavy walls with different wave lengths and amplitudes. The 2D and 3D topologies are defined by sinusoidal surface variation in one and two directions, $S_B=0.1cos(x\pi)$, and $S_B(x,y)=0.1cos(x\pi)cos(y\pi)$, respectively. Krettenauer and Schumamn (1992) performed DNS and LES of the same 2D configuration, though at a much lower Ra number of $Ra=5.5\times10^4$ and observed that the gross feature of the flow statistics, such as the profiles of turbulence variance and fluxes were not very sensitive to the variations of the bottom wall topology. On the other hand, the motion structure persisted considerably longer over the wavy terrain than over flat surfaces.

Fig. 4a shows the influence of the bottom wall topology on time evolution of integral Nusselt number for four different wall configurations: a flat bottom surface (conf1), a 2D wavy surface in x-direction (conf2), the same configuration with twice longer wave length (conf3) and a 3D topology (conf4). The 3D wave configuration promotes a fully developed regime earlier than others. The longer wave length in 2D surface configuration keeps the initial flow organisation for very long period of time (almost 200 nondimensional time units). When the fully developed stage was reached, the integral Nusselt number approached the value for the flat wall,

indicating that the imposed waviness of the bottom wall affects the integral heat transfer in fully developed stage only marginally.

Fig. 4b illustrates the effect of the 'subscale' model by comparing the 'pseudo DNS' (no subscale model) and TRANS. Both simulations show an almost identical time response in the development of the overall Nu number, in a close correlation with the behaviour of the maximum velocity components. The first peak is observed when the U and W velocity components reach their peak values for the first time (τ^*=15), followed by a decline until the V velocity reaches its maximum, followed by a subsequent increase in heat transfer. A relatively coarse mesh of $82^2 \times 32$ resulted in a laminar-like regime for the simulation without subscale model, and the averaged value of the overall Nu was 12. Contrary to this behaviour, the simulation with the ASM/AFM subscale model was able to promote the higher heat transfer yielding the final averaged value of Nu=18. According to Krettenauer and Schumann (1992), the total heat transfer in their simulations was just slightly affected by the wall waviness. The above obtained value of the Nu number confirmed the findings of Krettenauer and Schumann (1992), and stresses the importance of the subscale model in the range of low and transitional Ra numbers for complex geometries, when the grid resolution is not sufficient to resolve all scales.

The effect of the bottom wall configuration on the mean properties (W,T) and second moments ($\overline{\theta^2}$) is presented in Fig. 5a and Fig. 5b. At the initial stage of heating, τ^*=50, the contours of vertical velocity and temperature in the horizontal plane (x,y,0.5) show a regular flow pattern determined by the wall configuration, Fig. 5a. Updrafts are represented by solid lines and downdrafts by dashed line contours. The sites of the plume generation are located at the surface wave peaks, as observed by 5 plumes regularly extending in the vertical direction. At τ^*=200 the picture is significantly different. The locations of the plume realization are not fixed anymore, the two-dimensional structure orientation is lost, and the plume movement produces a strong horizontal motion. The second moments (the modelled part) show a similar behaviour: the contours of $\overline{\theta^2}$ in the vertical planes indicate that $\overline{\theta^2}$ are concentrated in the near-wall regions. This is what we expected, since the main role of subscale model is to produce a correct near-wall behaviour while in the outer region the large scales are resolved.

A similar analysis is performed for the 3D surface wave configuration. The plumes raise from the surface peaks and sink into the surface valleys, portraying 25 characteristic locations in (x,y,0.5) plane, Fig. 5b. At τ^*=200 the initial organisation of the flow cannot be observed anymore. Thermal plumes occupy a significantly larger space and not only the regions close to the bottom surface peaks, as found in the initial phase of flow development.

In order to get a better insight in the organisation and modification of the large coherent structures, we applied the structure identifying analysis to an instantaneous TRANS realization. Fig. 6 shows the time evolution and spatial organisation of large structures defined and identified by kinematic vorticity number, $\mathcal{N}_k$. Very different shapes and organisations are observed in the initial stage of heating (τ^*=50) for two different topologies of the bottom wall. The large two-dimensional structures extending in y-direction and located in the centre of the cavity are observed for the imposed 2D topology. Contrary to this, for 3D wave topology, the coherent structures are located in the near wall regions and are significantly smaller in size. At (τ^*=200), the structures are very similar in shape and size for both configurations, but even for this time instant, significantly different flow reorganisation can be observed (diagonally oriented for 3D topology and around the central y-axis for 2D wave topology). In both cases and at both time instants, a close correlations between thermal plumes and large structures can be observed.

CONCLUSIONS

The time-dependent Reynolds-averaged Navier-Stokes (TRANS) approach was applied to analyse the effects of the imposed Lorentz force and bottom wall waviness on the reorganisation of the large coherent structure in Rayleigh-Bénard convection at high Ra numbers. While fully resolving the large-scale motion, the single-point three-equation $k-\varepsilon-\overline{\theta^2}$ algebraic stress/flux model was used to compute the second-moments associated with the unresolved ('subscale') motion. The method was earlier validated for classical R-B convection over flat walls, showing very good agreement with DNS and experimental data. A major advantage of the method is in resolving the dominant large-scale transport, dispensing with a need to use gradient transport hypotheses. The approach is regarded as potentially useful for both the distributed and boundary control of turbulent flow, heat and mass transfer through the control of large coherent structure.

REFERENCES

Cortese, T. and Balachandar, S., 1993, Vortical nature of thermal plumes in turbulent convection. *Phys. Fluids, A*, Vol. 5, No. 12, pp. 3226-3232.

Kenjereš, S. and Hanjalić, K., 1998, Transient analysis of Rayleigh-Bénard Convection over flat and wavy walls with a RANS model, *Proc. Turbulent Heat Transfer 2*, Engineering Foundation Conference, May 31-June 5 1998, Manchester, U.K.

Kenjereš, S. and Hanjalić, K., 1999, Modelling the turbulent flow subjected to magnetic field, *Proc. 4th Int. Symp. Engineering Turbulence Modelling and Measurements* W. Rodi and D. Laurence, eds., Elsevier (in press).

Kerr, M. R., 1996, Rayleigh number scaling in numerical convection. *J. Fluid Mech.*, Vol. 310, pp. 139-179.

Kretenauer, K. and Schumann, U., 1992, Numerical simulation of turbulent convection over wavy terrain. *J. Fluid Mech.*, Vol. 237, pp. 261-299.

Mößner and Müller , 1999, A numerical investigation of three-dimensional magnetoconvection in rectangular cavities, *Int. J. Heat and Mass Transfer*, Vol. 42, pp. 1111-1121.

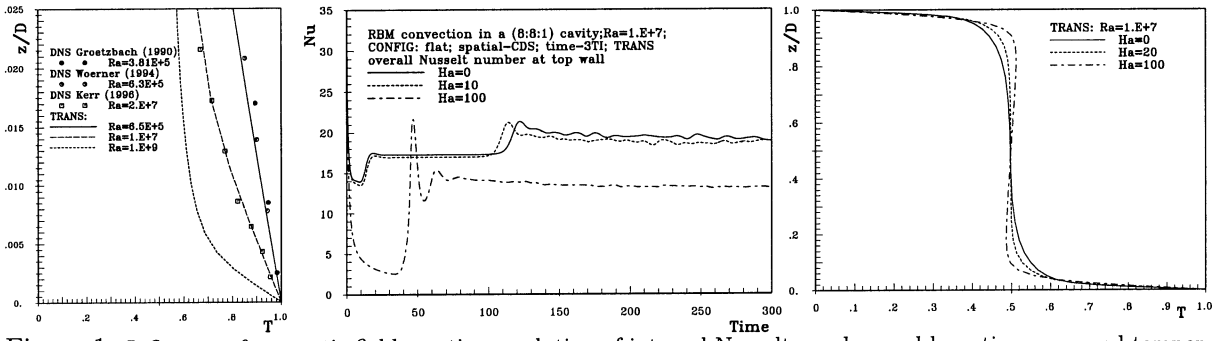

Figure 1: Influence of magnetic fields on time evolution of integral Nusselt number and long-time averaged temperature profiles

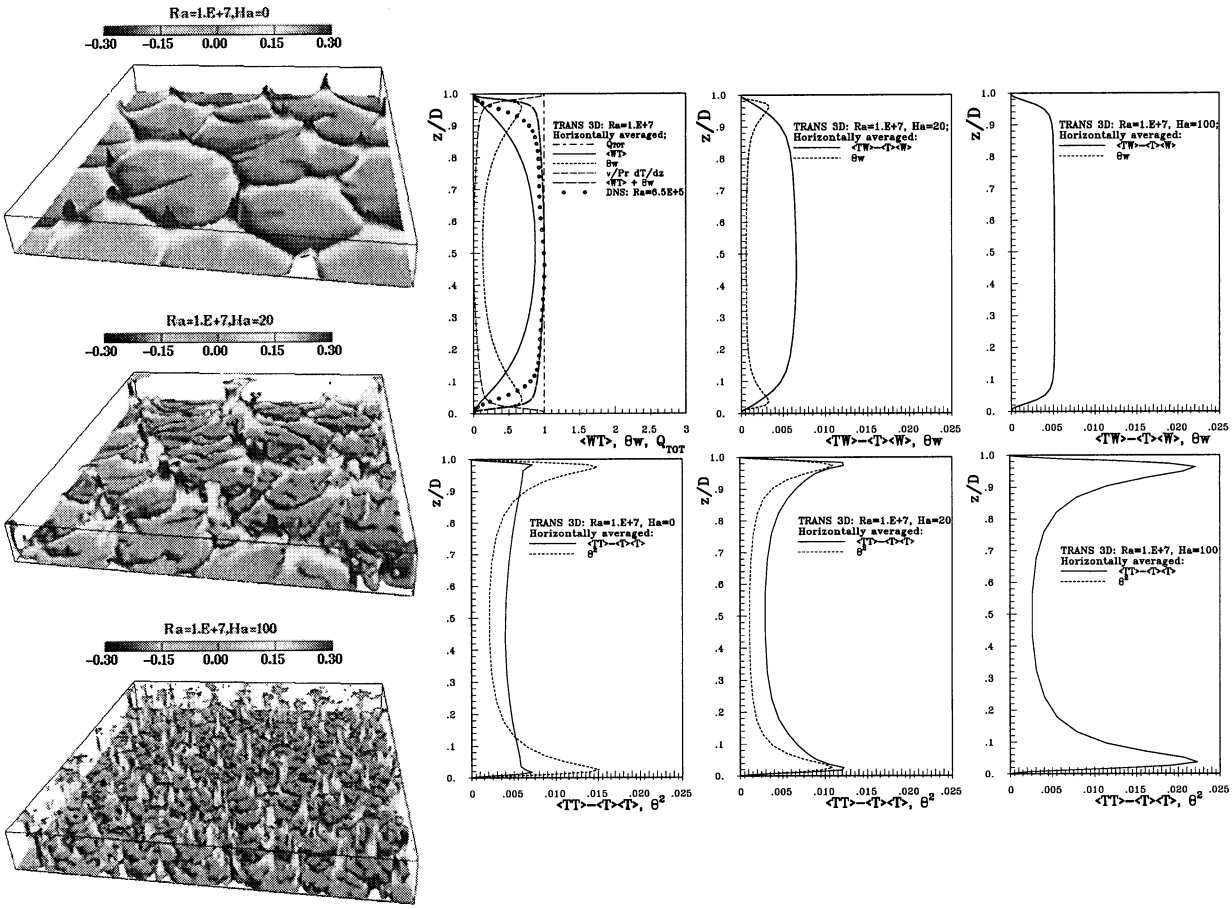

Figure 2: Effects of magnetic field on planform structures and resolved and modelled contributions of vertical heat flux and temperature variance

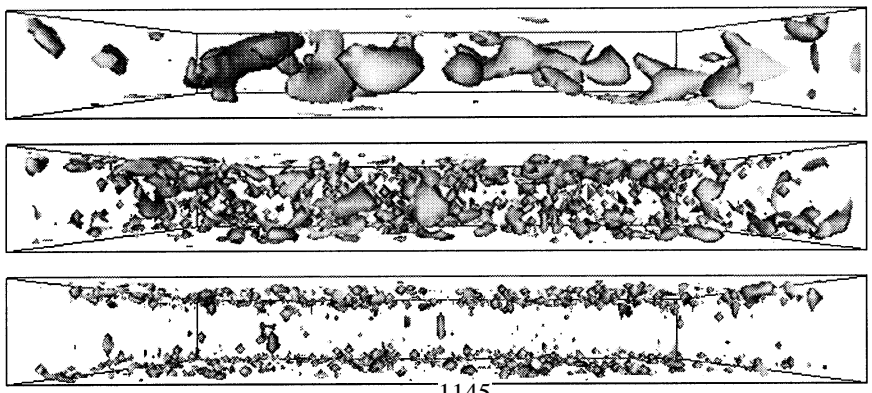

Figure 3: Influence of different magnetic fields on spatial reorganisation of large coherent structures defined by kinematic vorticity number, $\mathcal{N}_k = \left(|\omega_i|^2 / 2 S_{ij} S_{ij}\right)^{1/2} = 3$;

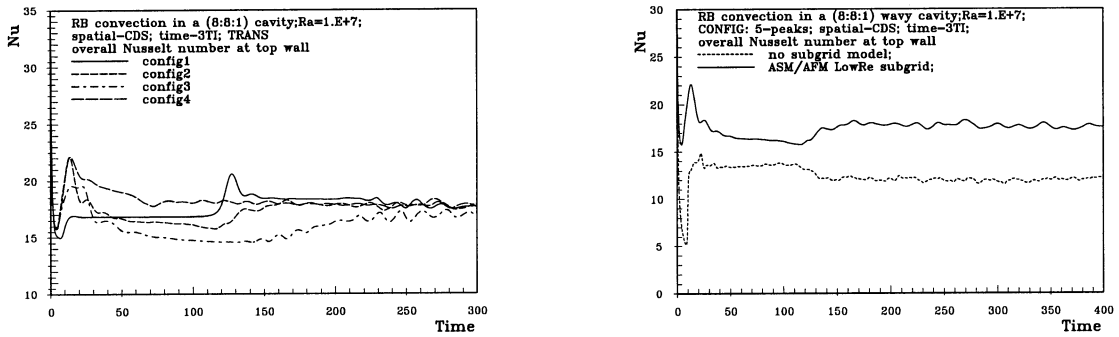

Figure 4: Influence of the bottom wall topology (left) and subscale model (right) on time evolution of integral Nusselt number

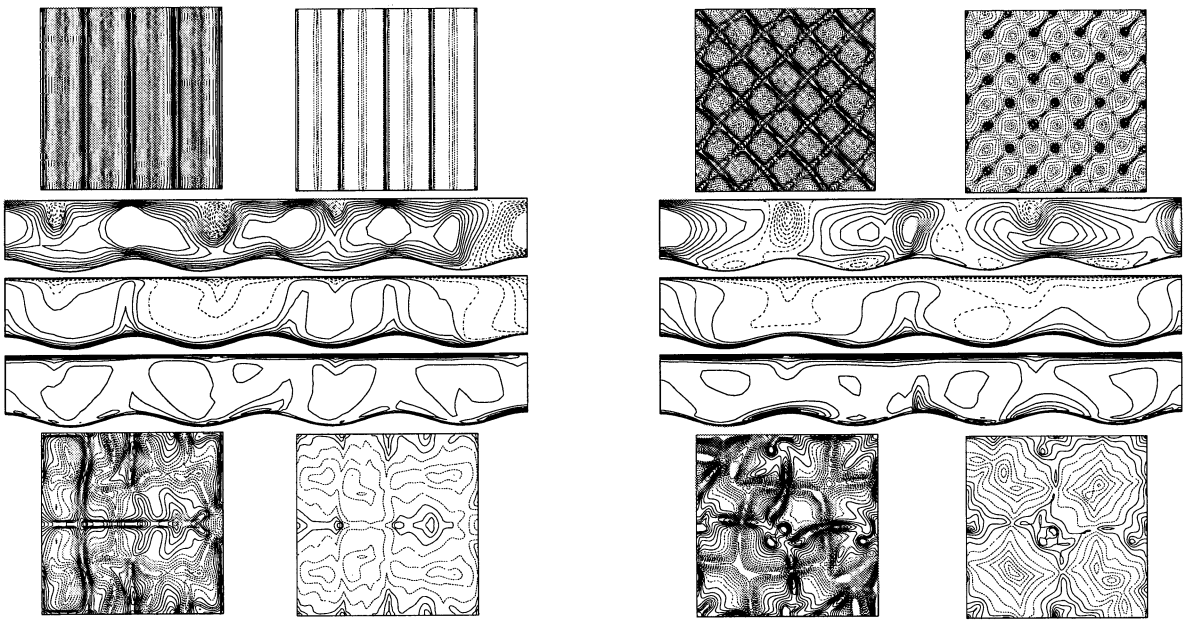

Figure 5: The effect of bottom wall configuration on first (W,T) and second order statistic ($\overline{\theta^2}$), left- S_B=$0.1cos(x\pi)$, right- S_B=$0.1cos(x\pi)cos(y\pi)$

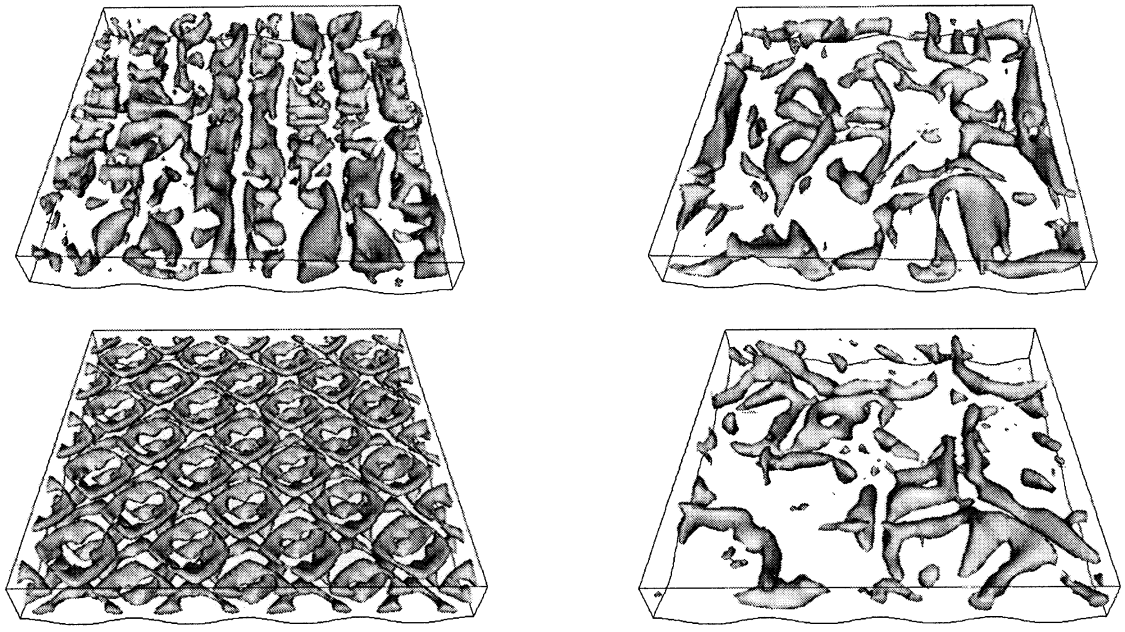

Figure 6: Time evolution and spatial organisation of large coherent structures defined and identified by $\mathcal{N}_k$=2, first column at τ^*=50, second column at τ^*=200, left- S_B=$0.1cos(x\pi)$, right- S_B=$0.1cos(x\pi)cos(y\pi)$